Analysis of Z_{eff} profiles based on space-resolved measurement of extreme ultraviolet bremsstrahlung in the Large Helical Device

X. L. HUANG[1], S. Morita[1,2], T. Oishi[1,2], M. Goto[1,2] and H. M. Zhang[1]

[1] *Department of Fusion Science, Graduate University for Advanced Studies, Toki 509-5292, Gifu, Japan*

[2] *National Institute for Fusion Science, Toki 509-5292, Gifu, Japan*

Abstract

Z_{eff} profile analysis has been carried out in a low-density and high-T_i discharge with carbon pellet injection. The evolution of the Z_{eff} profile shows a centrally peaked profile just after the pellet injection which then gradually returns to a flat profile. Comparison between the evolution of Z_{eff} and T_i profiles strongly suggests there is a positive relation between Z_{eff} and T_i.

I. Introduction

Study on impurities in fusion devices has been a major subject in fusion research because of the important role of impurities in plasma performance. The impurity content is commonly characterized by the effective ion charge $Z_{eff} = \sum_i n_i Z_i^2 / \sum_i n_i Z_i = \sum_i n_i Z_i^2 / n_e$. The value of Z_{eff} is known as a key parameter in increasing the ion temperature T_i of plasmas with neutral beam injection (NBI) in the Large Helical Device (LHD) [1,2]. Improvement of plasma performance including increase in T_i has been observed with carbon pellet injection [3]. Extremely hollow profiles of carbon impurity, denoted as "impurity hole", occur after the carbon pellet injection [4]. In order to understand the role in the process of plasma performance improvement, it is necessary to measure the radial distribution of Z_{eff} in the high T_i discharges.

Z_{eff} can be derived from the emissivity of bremsstrahlung, which is expressed by the following equation;

$$\varepsilon_{brem} = \frac{1.89\times10^{-28} n_e^2 g_{ff} Z_{eff}}{T_e^{1/2}\lambda^2} \exp\left(\frac{-12400}{T_e\lambda}\right), \quad (1)$$

where ε_{brem} (W·cm^{-3}·Å), n_e (cm^{-3}), g_{ff}, T_e (eV) and λ(Å) stand for the emissivity, the electron density, the free-free gaunt factor, the electron temperature and the wavelength, respectively.

A Czerny–Turner spectrometer has been installed on the LHD to measure the radial bremsstrahlung profile in the visible range [5]. However, the visible bremsstrahlung profile is strongly affected and distorted by bremsstrahlung emission from the edge boundary of the LHD ergodic layer in low-density discharges [6]. As the electron density in high T_i discharges is usually below 2×10^{13} cm^{-3}, it becomes difficult to obtain Z_{eff} profiles using the visible spectrometer. On the contrary, the bremsstrahlung in the extreme ultraviolet (EUV) range is free of the non-uniform edge bremsstrahlung emission because of the higher photon energy in the EUV range compared with that in the visible range. In addition, the bremsstrahlung is much stronger in the EUV range. Therefore, Z_{eff} profiles in high-T_i discharges can be evaluated from the space-resolved measurement of EUV bremsstrahlung.

II. Experimental setup

Two space-resolved EUV spectrometers have been installed on LHD [7,8]. Both spectrometers include an entrance slit, a spatial-resolution slit, a varied-line-spacing holographic grating and a charge-coupled device (CCD) detector with 1024×255 pixels. Time resolution of the two systems was 200ms in 2012 and has been improved to 50ms after the installation of a new CCD for each system in 2013. The vertical spatial resolution of the systems is roughly 3cm. One of the space-resolved spectrometer called "EUV-Short2" works in the wavelength range of 10-130Å, and can measure only upper half of the elliptical plasma, as shown in Fig. 1. The other spectrometer called "EUV-Long2" works in the wavelength range of 30-650Å, which can measure either upper or lower half profile. A 0.5μm-thick filter made of polyethylene terephthalate (PET) is installed in each system to reduce spike noises caused by high-energy NBI particles. The filter can effectively eliminate the spike noise. A spectrum measured by EUV-Long2 in a low density discharge is shown in Fig. 2. The continuum can be observed at the base line of the spectrum.

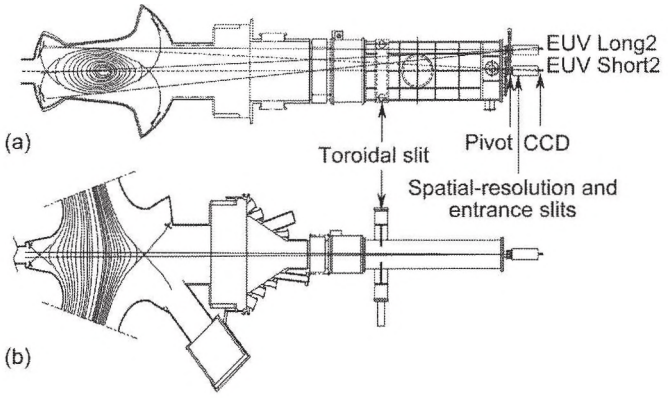

Fig. 1 (a) Side view and (b) top view of EUV systems on the LHD.

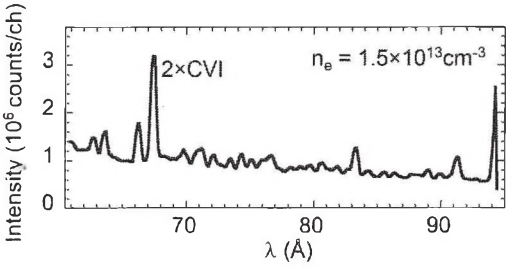

Fig. 2 EUV spectrum measured in a low-density discharge.

In order to obtain a better signal-to-noise ratio, the aperture size of the slits in the EUV systems are changed to 200 μm (width of entrance slit) × 2 mm (height of space-resolved slit), which is four and two times as large as the sizes of the usually used slits for EUV-Short2 and EUV-Long2, respectively. Consequently, new intensity calibration is necessary to obtain the absolute intensity. The EUV systems are calibrated by means of comparison between visible and EUV bremsstrahlung profiles. The visible bremsstrahlung profile has been measured by the above-mentioned Czerny–Turner spectrometer. Figure 3 shows the calibration results. Fitting with previous calibration curves are also plotted with solid lines. The calibration factor shows that the system brightness is enhanced by a factor of 4.0 and 2.2 for EUV-Short2 and EUV-Long2, respectively. This means the system brightness is approximately proportional to the size of the slit aperture.

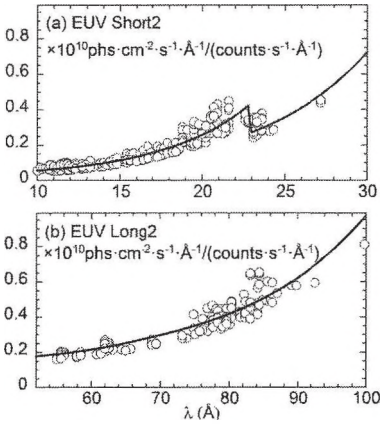

Fig. 3 Intensity calibration factors as a function of wavelength for (a) EUV Short2 and (b) EUV Long2. Solid lines denote fitting curves using previous calibration results.

III. Analysis of Z_{eff} Profile

A typical example of Z_{eff} profile analysis at λ = 77.4 Å -80.0 Å is shown in Fig. 4. The vertical profile of the line-integrated signal is plotted in Fig. 4(a) and radial profiles of n_e, T_e, ε and Z_{eff} are shown in Figs. 4(b)-(e), respectively. The emissivity profile, ε, is derived from the line-integrated profile based on Abel inversion. The magnetic surface used in the inversion is calculated with VMEC code [9]. The emissivity near the last closed flux surface (LCFS) is much larger than that in the plasma core ($\rho < 0.75$) as seen in Fig. 4(d). It seems that the large amount of continuum radiation is attributed to recombination radiation instead of bremsstrahlung because the intensity of bremsstrahlung is limited by Z_{eff}, which should be less than 6 if the impurity density is determined by only carbon. Since the photon energy is around 158 eV, the recombination radiation mainly originates in C^{4+} and C^{5+}. This is verified by comparison of the edge continuum emissivity profile and the carbon line emissions, C VI 33.73Å and C V 40.27Å+40.73Å, as shown in Fig. 4(d). The line emission profiles reflect the distributions of corresponding ions. The edge emissivity profile seems to be a superposition of the shapes of the two line emission profiles. Despite the large amount of recombination radiation in the edge, the emissivity profile is basically free of recombination radiation in the plasma core ($\rho < 0.75$) because of the following reasons. First, the enhancement of continuum emissivity due to recombination radiation dramatically decreases with increasing electron temperature [10]. For instance, the enhancement factor of recombination radiation caused by C^{5+} is around 12 at T_e = 0.2 keV while the factor decreases to 1.2 at T_e = 2 keV. Second, the impurity ions contributing to the observed recombination radiation, namely, C^{4+} and C^{5+}, are mainly located in the edge. Therefore, the emission from the plasma core certainly consists of only the bremsstrahlung.

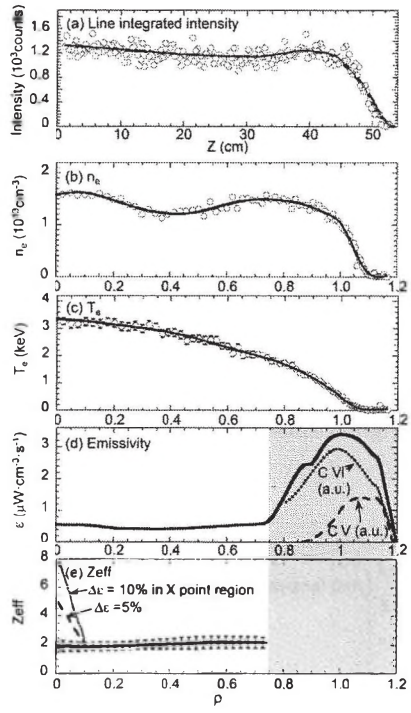

Fig. 4 (a) Vertical profile of line-integrated signal and radial profiles of (b) electron density, (c) electron temperature, (d) continuum emissivity at 77.4 Å-80.0 Å and (e) effective ion charge. Solid lines in (a)-(c) indicate curve fitting, and shaded area in (d) and (e) denotes the region affected by recombination radiation. Dashed and dotted lines in (d) denote shapes of C V and C VI emissions. Dashed and dotted lines in (e) indicate Z_{eff} deviation assuming strong emissions from the X point region.

In order to complete the Abel inversion, the magnetic surface obtained with the VMEC code is extrapolated to the region of $1 < \rho \leq 1.3$. If the bremsstrahlung continuum or impurity emissivity outside the LCFS is nonuniform in the poloidal direction, the measured line-integrated profile will be distorted. However, it is not the case in the EUV bremsstrahlung measurement because the energy is relatively high. The C^{4+} and

C^{5+} ions distribute around the LCFS where the connection length L_c is still quite long, e.g. $L_c > 10^3$ m. Therefore, the ion density can be considered to be uniform in the poloidal direction and then the resultant recombination radiation with such ions will be also uniform. This is verified by an impurity simulation in the ergodic layer [11]. A possible uncertainty caused by the recombination radiation from X points of the ergodic layer should be also taken into account. Assuming that the integrated emissivity outside the LCFS along a viewing chord of the spectrometer is enhanced by emissions from the X point region by a percentage of 5% or 10%, the Z_{eff} near plasma center increases abruptly, as shown in Fig. 4(e). This effect is sometime observed in the measurement. Fortunately, the X point region with relatively strong emissions is usually narrow in the vertical direction, usually within Z = ±5cm. Therefore, only the viewing chord passing through this narrow vertical region is affected by unnecessary emissions. It corresponds to the radial region of $\rho < 0.1$. In other words, the Z_{eff} profile can be always measured successfully in most radial ranges in the plasma core.

The error bars plotted in Fig. 4(e) is calculated from the data scattering involved in the line-integrated intensity, the electron density and the electron temperature. The total uncertainty is estimated to be 20% - 30%.

IV. Evolution of Z_{eff} Profile in High-T_i Discharges

Time evolution of the NBI port-through power P_{NBI}, n_e, T_e, T_i, the plasma stored energy W_p and the radiation power P_{rad} are shown in Fig. 5. The Z_{eff} profile analysis is performed in six time frames, designated as F1- F6 as denoted in Fig. 5. A carbon pellet is injected at t = 4.5s. The line-integrated density n_e increases from 1.0×10^{13} cm^{-3} to 2.2×10^{13} cm^{-3} after the pellet injection and then gradually decays to 1.4×10^{13} cm^{-3}. The electron temperature T_e is not significantly affected by the pellet. The ion temperature T_i increases from 3.1 keV to 4.2 keV and becomes higher than T_e after the injection (F2). The value of T_i is maintained at around 4.0 keV for 200 ms (F3). The decrease in T_i starts from t = 5.0s and becomes lower than T_e after t = 5.25s.

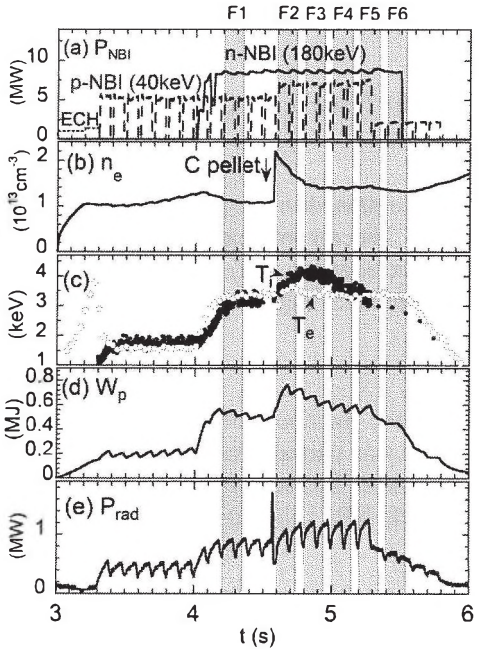

Fig. 5 Time evolution of (a) NBI port-through power, (b) electron density, (c) electron temperature and ion temperature, (d) plasma stored energy and (e) radiation power. Dashed areas indicate six time frames of F1-F6 used for the analysis.

The profiles of Z_{eff}, T_i and T_e in the above-mentioned time frames F1-F6 are shown in Fig. 6. The Z_{eff} profile is basically flat before the pellet injection. In the frame just after the injection (F2), the line-averaged Z_{eff} value increases by approximately 0.8 and a centrally peaked Z_{eff} profile occurs. At the same time, the T_i profile is increased as a whole and becomes higher than T_e in the central region ($\rho < 0.6$). All three profiles are maintained in the next time frame when the central T_i stays at 4.0 keV (F3). When the T_i starts to decrease at t = 5.0s, the Z_{eff} profile gradually returns to the original shape before the injection. The T_i profile tends to exhibit a similar behavior to Z_{eff} profile. The T_e profile remains basically unchanged in all

the time frames.

Comparison between the Z_{eff} and T_i profiles strongly indicates that there is a positive relation between Z_{eff} and T_i. Possible explanations are an enhancement of the absorption efficiency of NBI power and ion heating power per ion with increasing Z_{eff}. It has been also identified that the plasma confinement is improved in such high T_i discharges with carbon pellet injection. A recent study shows there is a strong relation between the density of the carbon impurity and the thermal diffusivity [12]. The time behavior of the Z_{eff} and T_i profiles also suggests that Z_{eff} plays an important role in the confinement improvement.

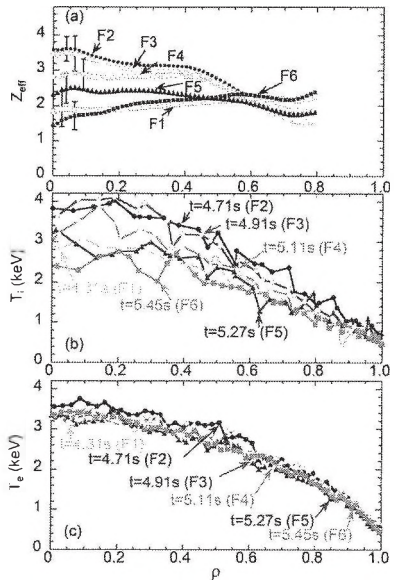

Fig. 6 Profiles of (a) Z_{eff}, (b) T_i and (c) T_e in the six time frames of F1-F6.

V. Summary

The Z_{eff} profile has been successfully obtained in the plasma core ($\rho < 0.75$) from space-resolved profiles of bremsstrahlung in the EUV range. The recombination radiation can give a significant effect on the bremsstrahlung profile, in particular, in the edge region ($\rho > 0.75$) and also in a small region ($\rho < 0.1$) near the plasma center. The time behavior of Z_{eff} profiles suggests a strong relation between Z_{eff} and T_i.

Acknowledgements

The authors would like to thank all the members of the LHD experiment group for their cooperation including technical support. This work was partially carried out under the LHD project financial support (NIFS14ULPP010) and also partly supported by the JSPS-NRF-NSFC A3 Foresight Program in the field of Plasma Physics (NSFC: No.11261140328, NRF: No. 2012K2A2A6000443).

References

[1] H. Takahashi *et al.*, Nucl. Fusion **53**, 073034 (2013).
[2] Y. Takeiri *et al.*, Nucl. Fusion **45**, 565 (2005).
[3] S. Morita *et al.*, Plasma Sci. Technol. **13**, 290 (2011).
[4] M. Yoshinuma *et al.*, Nucl. Fusion **49**, 062002 (2009).
[5] H. Y. Zhou *et al.*, Rev. Sci. Instrum. **79**, 10F536 (2008).
[6] H. Y. Zhou *et al.*, Rev. Sci. Instrum. **81**, 10D706 (2010).
[7] C. F. Dong *et al.*, Rev. Sci. Instrum. **81**, 033107 (2010).
[8] X. L. Huang *et al.*, Rev. Sci. Instrum. **85**, 043511 (2014).
[9] K. Yamazaki, J. Plasma Fusion Res. **79**, 739 (2003).
[10] E. H. Silver, *et al.*, Rev. Sci. Instrum. **53**, 1198 (1982).
[11] E. H. Wang, *Development of two-dimensional EUV spectroscopy for study of impurity behavior in ergodic layer of LHD* (The Graduate University for Advanced Studies, 2013) p.111-p.115.
[12] M. Osakabe *et al.*, Plasma Phys. Control. Fusion **56,** 095011 (2014).